Secondary particle size determining sedimentation and adsorption kinetics of titanate-based materials for ammonia nitrogen and methylene blue removal

Wenlong Zhang[a,1], Changjiang Huo[b,1], Bo Hou[c], Changzheng Lin[a], Xuanye Yan[a], Jiangtao Feng[a,*], Wei Yan[a]

[a]Department of Environmental Science and Engineering, State Key Laboratory of Multiphase Flow in Power Engineering, School of Energy and Power Engineering, Xi'an Jiaotong University, Xi'an 710049, China

[b]Department of Fluid Machinery and Engineering, School of Energy and Power Engineering, Xi'an Jiaotong University, 28 West Xianning Road, Xi'an, China, 710049

[c]School of Physics and Astronomy, Cardiff University, The Parade, Cardiff, CF24 3AA, Wales, UK

Abstract

The effect of the main size distribution of particles on the adsorption process for adsorbent materials has been well-recognized; however, the impact of secondary particles size (agglomerated, aggregated or hydrated ones) on adsorbent properties and performance was rarely reported so far. In this study, a series of sodium titanates (STs) and peroxide modified sodium titanates (PSTs) with different primary particle sizes, and secondary sizes are synthesized by controlling synthesis conditions and

*Corresponding author.

E-mail address: fjtes@xjtu.edu.cn

[1]These two authors contributed equally to this paper.

subsequently applied to batch adsorption experiment. By employing scanning electron microscopes and Laser particle size analyzers, the particle size of STs and PSTs are found to be closely correlated with synthesis conditions. The surface morphology and specific surface area of titanates are size-dependent, while the components of all the samples maintained constant. The sedimentation experiment and CFD simulation demonstrated that particles with larger secondary sizes tended to settle more quickly than those with a bigger sizes. PSTs or STs particles with smaller secondary sizes could reach equilibrium more rapidly than those with the bigger size. The fitting results from Elovich and Weber-Morris models demonstrated that the particles size affect kinetics mainly through the liquid film diffusion process within the initial stages.

Keywords: Titanate**;** Secondary size**;** Sedimentation; Adsorption; Water treatment

1. Introduction

Recently, there has been considerable concerns about emerging threats from the total nitrogen (TN) and chemical oxygen demand (COD) in water and other ecosystems [1, 2]. The removal of ammonia nitrogen (NH_4^+) or methylene blue (MB) from wastewater has drawn much attention in water purification due to their great contribution to TN or COD pollution, respectively [3, 4]. Adsorption, one of the practical and popular physicochemical techniques used in water treatment, has been frequently employed for removing NH_4^+ and MB because of its high efficiency, cost-effective and easy operation [5, 6]. Numerous studies have been carried out to understand the adsorption process [7]. It has been widely demonstrated that solution pH, environment temperature or contact time, and the properties of an adsorbent such as surface charge, functional groups, or pore structure can significantly impact the adsorption performance[8-12]. However, the particle size effect on the adsorbent properties and adsorption process is less still unclear, even though most adsorbent materials for NH_4^+ or MB are powders or particles in nature [13, 14]. It has been shown that many fundamental properties of powder materials like mechanical and electrical performance are size-dependent when the diameter of particles are nanoscale [15]. Indeed, particle size change could impact the movement of particles in solution according to the Brownian motion. In addition, the particle size of materials could also

affect the value of surface free energy and then might have effects on the adsorption interaction [16].

It has been found that the adsorption of MB onto diatomite is size-dependent when the size scale is larger than 250 μm, and the maximum uptake capacity decreases with the reduction of size. The same phenomenon was found in the adsorption of bisphenol A onto montmorillonite [16, 17]. However, the particle size value discussed in most reports was determined directly from SEM image or sieve action, which could not show the actual scale of particles in solution because of aggregation [18]. The size of solid materials in an aqueous environment could be described through two different approaches: the primary size for individual particles and the secondary size for agglomerated, aggregated or hydrated particles [19]. Therefore, the secondary size value is closer to the actual conditions and appropriate for the size-dependent discussion.

Titanate, one of the common inorganic ion-exchange adsorbents or photocatalysts [20, 21], was chosen as the main adsorbent for size dependence experiment according to the following two merits: 1) amorphous sodium titanate (ST) and peroxide modified sodium titanate (PST) particles can be facilely synthesized through only mild hydrolysis method. The secondary particle size can be easily controlled for ST and PST by changing synthesis conditions such as the ratio and concentration of reagents. 2) Titanate based materials exhibit excellent adsorption efficiency for cationic contaminants due to their ion-exchange ability demonstrated by literature [22-25].

In this study, NH_4^+ and MB were chosen as the targeted contaminants not only because of their contribution to TN and COD but also due to their large difference in

molecular weight and size, which might help uncover the relation between particle size dependence and adsorbate molecular properties. Several challenges in secondary particle size-dependent sedimentation and adsorption kinetics of titanate-based materials for ammonia nitrogen and methylene blue removal have been systematically studied: 1) a series of titanates named sodium titanates (STs) and peroxide modified sodium titanates (PSTs) with different particle sizes were facilely synthesized by changing synthesis conditions. 2) The effect of titanates particle secondary size on adsorbent properties and adsorption performance in removal of NH_4^+ or MB were conducted and discussed. 3) The potential mechanisms of the effect of particle size were also revealed.

2. Experimental procedures

2.1. Materials

TIPT (titanium isopropoxide, $Ti(OC_3H_7)_4$), H_2O_2 (hydrogen peroxide, 30 wt%), NaOH (sodium hydroxide), HCl (hydrochloric acid), anhydrous ethanol(99.7%), HDA (hexadecylamine, 90 wt%) and isopropanol were of analytical reagent grades and used without any further purification. The simulated wastewater used in this study were obtained by dissolving ammonium chloride (NH_4Cl, GR) or methylene blue (MB, BS, Fig. S1) (both from Sinopharm Chemical Reagent Co. Ltd, China) into deionized water. The deionized water used for all the experiments was prepared by an EPED-40TF Super pure Water System, China.

2.2. Synthesis of titanate samples

A series of sodium titanates (STs) with different particle sizes were prepared based on our previous study [22]. The particle size of STs powders was adjusted by controlling the hydrolysis rate of TIPT, where the volume of H_2O was changed according to the molar ratio of TIPT: H_2O (1:1, 1:10, 1:20). HDA was served as a structure-directing agent [26]. In a typical synthesis procedure, 0.8 g of NaOH and 2 g of HDA were dissolved in a mixed solution of 200 mL ethanol and a certain amount of H_2O (0.61, 6.10 and 12.2 mL) with agitation at ambient temperature. 10 mL of TIPT was added dropwise into the above solution under stirring. After 24 h, the white suspension was recovered by centrifugation. The solid sample was washed with ethanol five times and dried at 60˚C for 12 h [27]. The as-prepared white samples were labelled as ST (1:1), ST(1:10) and ST(1:20) according to the TIPT: H_2O molar ratio. All the samples were further purified by the sieve with 200 mesh.

A series of peroxide modified sodium titanate (PSTs) with different particle sizes were synthesized as follows: a mixture of TIPT (10 mL) and isopropanol with the volume ratio of 5:2 was added into 200 mL NaOH solution (0.1 $mol \cdot L^{-1}$) with magnetic stirring at 60˚C [28]. Afterwards, an appropriate amount of H_2O_2 (5 mL, 10 mL and 20 mL respectively) was dropwise added into the white suspension in 1 h, accompanied by stirring. The solution gradually became transparent and bright yellow, and then the yellow suspension was stirred for another 30 min at ambient temperature. The yellow solid was filtered out and subsequently washed with deionized water until the filtrate pH reached approximately 7.0, then dried at 60 ˚C for 12 h. The as-prepared PST samples were denoted as PST-5, PST-10 and PST-20 according to the volume of H_2O_2

used in the synthesis process, respectively. All the samples were sieved by the sieve with 200 mesh.

2.3. Analysis and characterization methods

The morphology of samples was investigated by scanning electron microscopy (SEM, MAIA3 LMH, US). The imaging and elemental mapping were performed using acceleration voltages of 15 kV. The element's contents of powder samples were measured by X-ray Fluorescence (XRF, Bruker S8 Tiger, Germany) without any pretreatment. The sample's secondary size in solution was determined by a laser particle size analyzer (LS-909, China). The actual density of samples was tested by a Gas Displacement Pycnometer (AccuPyc II 1340, US). The surface functional groups of adsorbents were identified by a Fourier transform infrared spectrometer (FTIR, Bruker, Germany) with the KBr pellet method at the wavenumber ranging from 400 to 4000 cm^{-1}. The Brunauer-Emmett-Teller specific surface area (S_{BET}) and pore structure characteristics of samples were determined by the Builder SSA-4300 (Beijing, China) at 77 K using the Barrett-Joyner-Halenda (BJH) method. The zeta potentials of the samples were measured with Brookhaven 90plus Zeta, samples of which (1.0 mg) were added into 10 ml NaCl solution (10^{-3} $mol \cdot L^{-1}$) at different pH values (adjusted by 0.5 $mol \cdot L^{-1}$ HCl and NaOH solution).

The control experiment was conducted to evaluate the property of as-prepared materials in solution as follows: 0.5 g of powders were added into a measuring cylinder with 25 mL deionized water and dispersed under ultrasound sonication for 30 min.

Afterwards, the cylinder with PSTs or STs solution was put on the surface of a flat desk, respectively. The photos were taken at different time intervals.

2.4. Numerical simulations

In the present study, Computational Fluid Dynamics (CFD) was also conducted to reveal the relationship between settlement property and particles size. Considering the symmetry of the test tube, a 2D axisymmetric domain with a height of 200 mm and a width of 20 mm was employed. Structured grids were firstly generated for the computational domain through software ICEM. Then, based on the finite volume method, numerical simulation was carried out using the software ANSYS-Fluent to analyze unsteady flow behavior. The Eulerian multiphase model was utilized to model granular flow, allowing two phases to share a single pressure and momentum, and continuity equations are solved for each phase [29]. The phase coupled SIMPLE algorithm was used for the pressure-velocity coupling scheme. The velocities were calculated coupled by phases in a segregated method, and the pressure correction equations were established based on total continuity. According to ANSYS-Fluent theory guide, the k-ε dispersed turbulence model was applicable when there is one primary continuous phase, and the rest are dispersed dilute secondary phases. Thus, the k-ε dispersed turbulence model with standard wall function was adopted to close the turbulence terms in the simulation. Moreover, the gravitational acceleration was specified as 9.81 m/s^2 to consider the gravity, and the Gidaspow method [30] was implemented for the drag law. The thickness of the initial particle layer was set as 5 mm

with a volume fraction of 0.2. The models with different particle diameters and densities were constructed to study their effect on the setting ability.

2.5. Adsorption experiments

Unless otherwise stated, NH_4^+ and MB removal experiments were performed at 25˚C in a temperature-controlled shaker with a 200 rpm stirring rate. The initial concentration of NH_4^+ and MB were 45 and 275 $mg \cdot L^{-1}$, respectively. The suspensions after adsorption were filtered in syringes equipped with 0.45 μm cellulose acetate membrane filters.

To investigate the effect of the solution pH on the adsorption of pollutants, 0.4 g of as-prepared STs or PSTs separately mixed with 20 mL individual NH_4^+ or MB solution at different pH values ranging from 2.0-12.0 (adjusted by either HCl or NaOH) in 50 mL centrifugal tube. The above solution was shaken for 120 min.

Adsorption kinetic experiments were carried out in a conical flask by adding 0.2 g of adsorbent into a 100 mL solution containing NH_4^+ or MB with initial pH of 7.0. At various time intervals, 1.5 mL suspension was withdrawn and filtered for determination.

Adsorption isotherms experiments were performed as follows: 0.04 g of each adsorbent (PSTs and STs) was added into a 50 mL centrifuge tube containing 20 mL solution with different initial concentrations varying from 10 to 160 $mg \cdot L^{-1}$ for NH_4^+, 50-300 $mg \cdot L^{-1}$ for MB at pH=7.0. The mixture was shaken at ambient temperature for 120 min.

The NH_4^+ concentration remaining in the solution was determined by the conventional salicylate spectrophotometric method. The MB concentration in solution was determined by a direct UV-Vis spectrophotometry method at a wavelength of 665

nm. The amounts of adsorbates adsorbed on the as-prepared STs or PSTs at a certain time Q_t (mg·g^{-1}) and equilibrium Q_e (mg·g^{-1}) were calculated by Eqs. (1)-(2). The adsorption efficiency R (%) was calculated by Eq. (3). Where C_0 (mg·L^{-1}) is the initial concentration of adsorbates, C_t (mg·L^{-1}) and C_e (mg·L^{-1}) are the residual adsorbate concentration at time t (min) and equilibrium; m (g) is the mass of adsorbent and V (L) is the solution volume. As shown in Eqs. (S1)-(S6), four kinetic models (pseudo-first order, pseudo-second order, elovich and web-morris models) and two isotherms models (Langmuir and Freundlich models) were used to analyze the adsorption data [31-33].

$$Q_t = \frac{C_0 - C_t}{m} \times V \tag{1}$$

$$Q_e = \frac{C_0 - C_e}{m} \times V \tag{2}$$

$$R = \frac{C_0 - C_t}{C_0} \times 100 \tag{3}$$

3. Results and discussion

3.1. Structure and morphology analyses

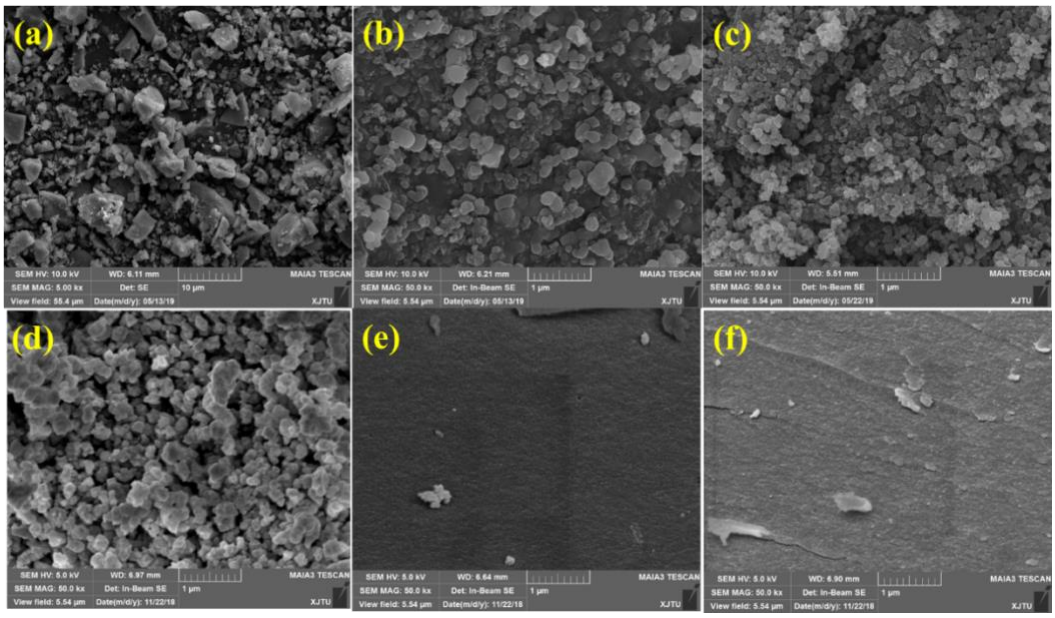

Figure 1. SEM images of ST (1:1) (a), ST (1:10) (b), ST (1:20) (c), PST-5 (d), PST-10 (e) and PST-20 (f).

The morphology of the primary size samples was analyzed by SEM, as shown in Fig. 1. It is observable that the diameter of granules in STs (Fig. 1a-c) decrease with the increase of H_2O volume in the synthesis procedure. The reduction of the Ti/H_2O molar ratio increased the hydrolysis rate of Ti precursor and cut down the production of large particles [34]. The average primary size of ST(1:1), ST(1:10) and ST(1:20) is about 500 nm, 300 nm and 150 nm, respectively. Agglomeration occurs primarily on the surface of ST(1:20) because the size of nano-particles is small [35]. The change of particles size and morphology in STs might affect the sample properties like surface area and the adsorption behavior in the aqueous phase [16]. The effect of synthesis condition on the morphology of PSTs is more significant than that of STs, as shown in Fig. 1d-f. The complexation reaction between H_2O_2 and Ti^{4+} can be affected by increasing H_2O_2 content during synthesis and result in different morphology and particles size [36]. It can be seen that the images that PST-5 (prepared with 5 mL H_2O_2) still maintains a rough surface consisting of particles like STs. However, PST-10 and PST-20 exhibit a well-organized morphology with tiny drapes and fewer particles, which might have a negative effect on the pore volume and specific surface area of samples. All the above results suggest that the modification process succeeded in changing the primary size of samples, favouring the modulation of secondary size in the aqueous phase.

Though the primary size is influential on the property of the sample, the secondary size of powder samples is possibly more significant when served as adsorbents in the aqueous phase [19]. The actual particles size (secondary size) of STs and PSTs owing

to agglomeration or hydration in agitating solution was measured by a Laser particle size analyzer and shown in Table 1. It is illustrated that the secondary size of samples is greatly different from the primary size of SEM images. The results also indicate that secondary particle size of STs and PSTs are in the order of ST(1:1)> ST(1:10)> ST(1:20) and PST-20> PST-10> PST-5, respectively. Controlling the hydrolysis rate (for STs) and complexation degree (for PSTs) successfully caused the difference in secondary particle size. It is also indicated from Table 1 and Fig. S2 that the surface area and pore volume of STs vary with the particle size value. The reduction of particle diameter resulted in an order of specific surface area as ST(1:20)> ST(1:10)> ST(1:1) and PST-5> PST-10> PST-20. However, the surface area value of PSTs is relatively low because the addition of H_2O_2 could effectively break the morphology of samples and reduce the number of pores. In addition, the XRF result (Table 1) demonstrated that the distribution of the element of STs or PSTs was hardly affected by the synthesis procedure.

Table 1. Physical-chemical properties of STs and PSTs by BET, XRF and Laser particle size analyzer.

Samples	ST(1:1)	ST(1:10)	ST(1:20)	PST-5	PST-10	PST-20
D_{50}/μm	89.13	72.78	53.56	62.81	76.59	92.40
D_{90}/μm	200.21	166.92	131.99	149.99	174.27	211.18
ρ/g·cm^{-3}	2.48	2.77	2.60	3.05	2.98	3.06
S_{BET}/m^2·g^{-1}	55.2	73.56	139.2	6.9	1.36	0.85
V/cm^3·g^{-1}	0.30	0.22	0.52	0.06	0.03	0.03
R_{pore}/nm	10.7	5.9	7.5	16.7	40.7	72.5
Ti/wt%	64.6	63.9	63.2	66.3	64.5	63.6
O/wt%	26.3	28.7	29.7	27.7	28.8	30.2
Na/wt%	7.1	7.4	7.1	6.0	6.7	6.2

It is evident from FTIR spectra of STs (Fig. S3a) and PSTs (Fig. S3b) that the typical peak responding to Ti-O-Na^+ (Ti-OH destroyed in the alkaline environment [37]) in 1340 cm^{-1} remains unchanged in these samples. Meanwhile, the peak responding to the Ti-O bond at about 900 cm^{-1} appears in PSTs and becomes stronger in the PST-10 and PST-20, which accounts for the coordination between the Ti-O framework and Na^+ instead of bridge connection[38]. During the PSTs synthesis, Na^+ might enter into the interior structure and made the sample's surface more negative in solution [36], which is meaningful for the adsorption of positive pollutants like cationic dyes. In addition, it is observed that Ti-O-O bonds (responding to 680 cm^{-1} peak [39]) appears in PSTs after the modification by H_2O_2, which might increase the acidity of the surface and promote attracting cations. In addition, the zeta potential results (Fig. S4a-b) show that the pH_{iep} (pH at isoelectric point) of ST(1:1), ST(1:10), ST(1:20), PST-20, PST-10 and PST-5 are 1.58, 2.01, 2.23, 1.15, 1.52 and 2.33, all of which are in low pH range. It is acceptable that the change of synthesis conditions only brought about a slight difference in the surface charge distribution. Therefore, the surface of STs and PSTs samples in solution would be negatively charged in a wide range of pH, which is beneficial for the cationic contaminants adsorption behavior [40].

3.2. Sedimentation property/adsorbent separation

The sedimentation property of adsorbent powders can reflect their separation tendency or affinity from the water after the adsorption process [41]. It is well known that some theoretical formulas are describing the sedimentation velocity of a spherical particle in a static solution, like the Stokes equation for the laminar region and Newton

equation for the turbulent region [42]. A meaningful conclusion can be made from these equations that the diameter and density of sphere particles could affect the sedimentation process. However, these ideal or empirical equations sometimes can't perfectly predict the sedimentation of powders because the actual environment is complicated. Therefore, the sedimentation experiment and CFD simulation are necessary for analyzing the role of particle size in sedimentation. The density and secondary size of as-prepared ST and PST samples have been changed through controlling the synthesis conditions and are showed in Table 1. It is evident that the density of PST samples is different from STs though the density value among PSTs or STs is similar. The setting experiment evaluated all the samples' setting properties, and the resulting photos are shown in Fig. S5. It can be seen that the settling velocity of PSTs or STs particles changes significantly with the change of synthesis conditions. The setting ability of these samples are in the order of ST(1:1)> ST(1:10)> ST(1:20) and PST-20> PST-10> PST-5, which is consistent with the order of secondary size.

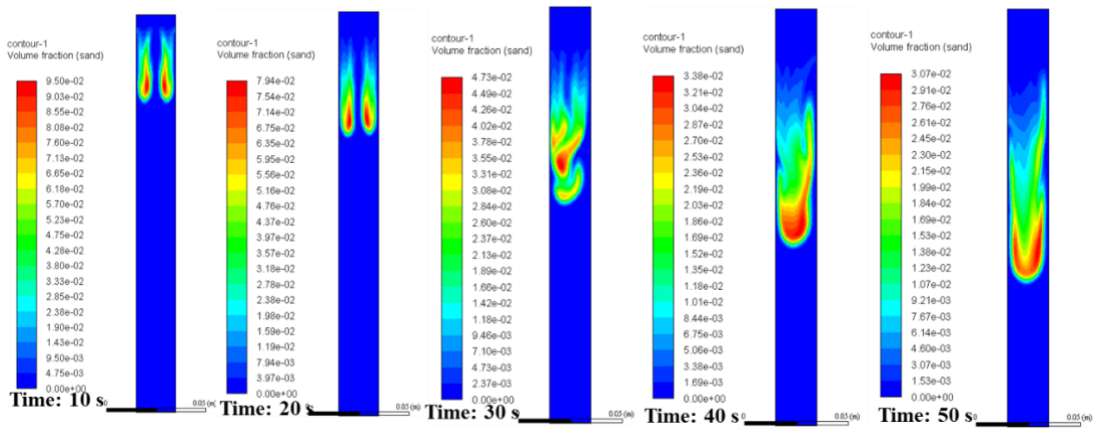

(a) ST(1:1)

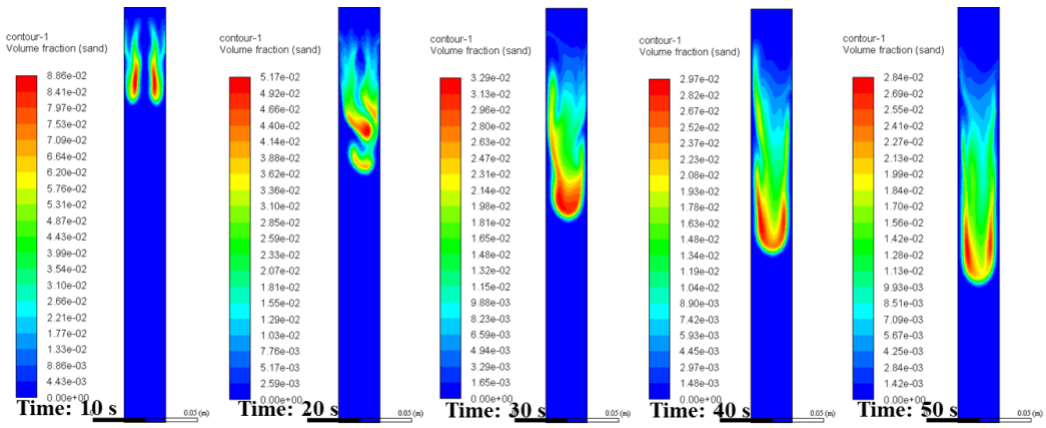

(b) ST(1:10)

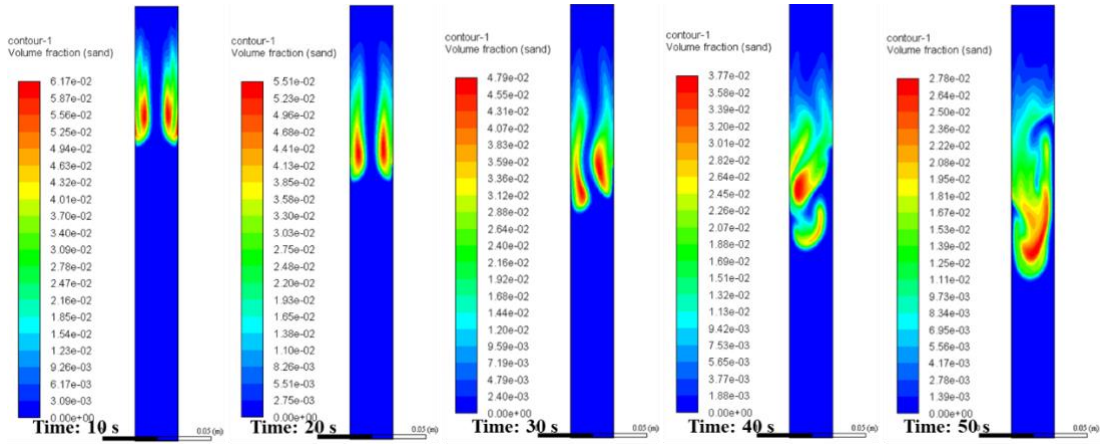

(c) ST(1:20)

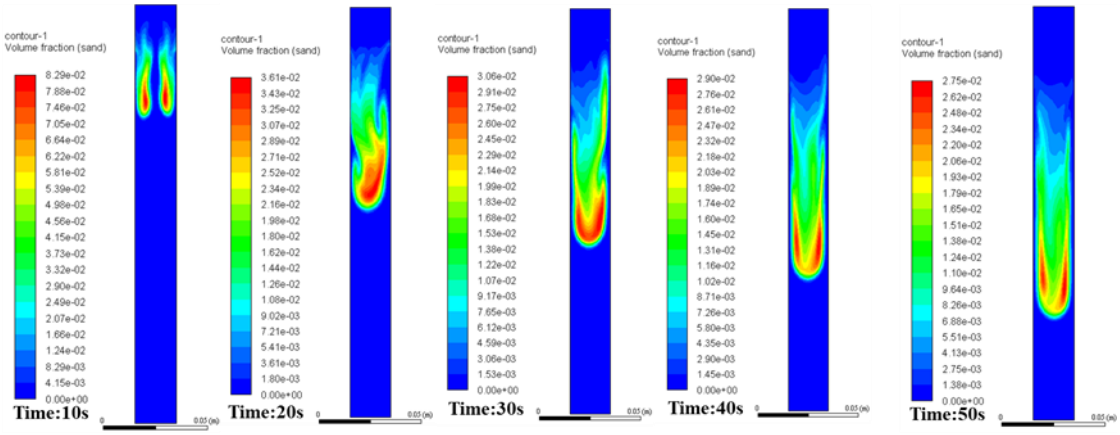

(d) PST-5

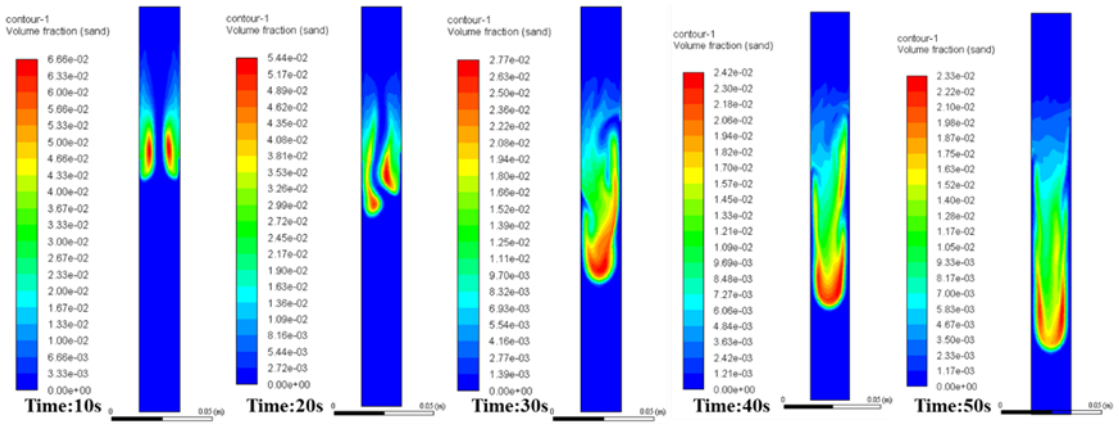

(e) PST-10

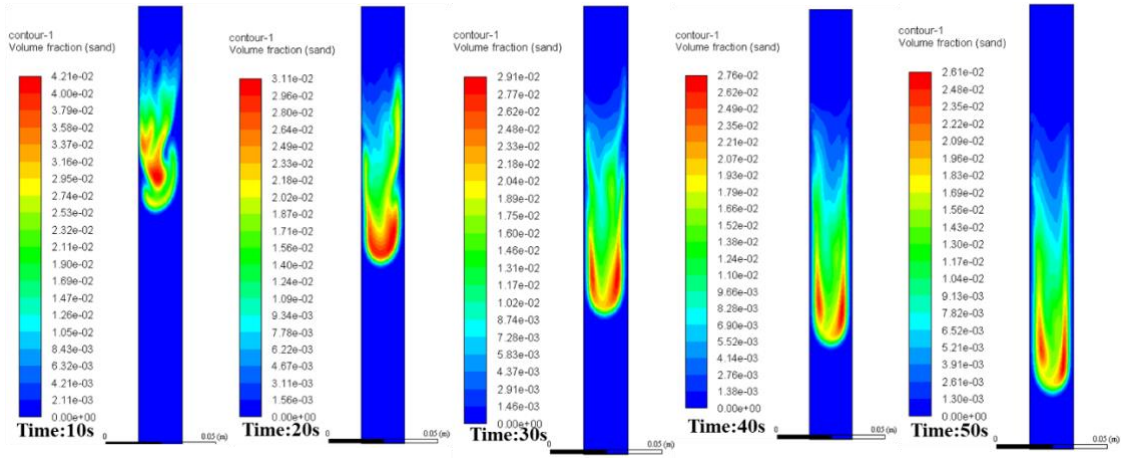

(f) PST-20

Figure 2. The simulation results of the setting process of STs and PSTs samples by Ansys-Fluent.

The simulation by CFD was also conducted to figure out the effect of secondary size and density on the setting ability of adsorbent particles. The numerical method is showed in section 2.4, and the parameters of particles were set according to the results in Table 1. For convenience, diameter D_{50} and average true density ρ were used to represent the chaotic state of actual particles in solution. On this basis, the simulation of the settlement process of these samples is showed in Fig. 2. The simulated settling conditions of STs or PSTs are consistent with the actual state, as shown in Fig. S5, which demonstrates the rationality of the numerical and simplification method. In

addition, we found that smaller particles tend to interact with others in a longer time than the larger ones in the initial phase of the settling process. The phenomenon can be attributed to the fact that the diffusion movement of particles with smaller sizes is stronger than particles with larger sizes due to the Brownian movement [43]. From Table 1 and Fig. 2, sample particles with larger density (PSTs) settle more easily and quickly than the small ones (STs). However, for the same kind of samples whose synthesis procedures are identical, the true density value of particles are similar. Thus, the main factor that affects the settling process is only secondary particle size. Therefore, controlling the diameter of particles through finitely changing synthesis conditions can effectively enhance or reduce the settlement ability of samples, which is meaningful for regulating the separation ability of saturated adsorbent materials.

3.3. Adsorption results

3.3.1. Effect of pH

Usually, the initial solution pH in adsorption experiments is one of the remarkable influence factors since the surface property of adsorbents and the form of adsorbate are pH-dependent [44, 45]. It is illustrated that the adsorption capacity of NH_4^+ onto STs or PSTs reached the maximum when the initial solution pH is 3~4 (Fig. S6a-b). The adsorption capacity of MB onto these adsorbents increased along with the increase of initial solution pH (Fig. S6c-d). The above results can be explained with the following two reasons: firstly, MB is cationic in all the tested pH ranges, and ammonia nitrogen is mainly cationic in the solution pH< 7 (NH_4^+); secondly, the STs and PSTs samples could be negatively charged at a large pH range according to the zeta potential

results [46]. In addition, considering the conclusion from the above characterization, the only particle size of samples is highly affected by synthesis conditions, but the particles' size has little effect on the adsorption capacity of NH_4^+ and MB by STs or PSTs. The adsorbent samples with smaller particle sizes possess a slight better adsorption performance at the same pH value. However, it is also indicated that the optimal pH value for the adsorption behavior of STs or PSTs is kept constant among different samples, which means that the particle size of the adsorbent sample is irrelative to the pH adaption.

3.3.2. Adsorption isotherms

The adsorption isotherm experiments of NH_4^+ and MB onto samples were conducted to find the effect of particle size on adsorption behavior with a series of initial solution concentrations. It is observable that the difference in particle size has a more powerful impact on MB adsorption than NH_4^+ for the same adsorbent material (please see Fig. S7). In addition, the difference in adsorption capacity for the same contaminant among the three PST samples is higher than that among the STs. The above results demonstrate that the effect degree of particle size on adsorption performance is relative to the property of both adsorbent and adsorbate. The diagram also indicates that smaller particle size is favorable for adsorption when other conditions remain constant. For instance, the adsorption of MB on STs is in order of ST(1:20)> ST(1:10)> ST(1:1). The increasing specific surface area and more intensive diffusion movement for smaller size samples might provide more active adsorption sites and contacts.

Two typical isotherm models (Langmuir and Freundlich model) were employed to fit the experimental data to understand the effect of particle size on the adsorption process and evaluate the adsorption performance. The nonlinear fitting curves were plotted in Fig. S7a-d, and a list of corresponding parameters was showed in Table 2. The correlation coefficients (R^2) value reveals that the Langmuir model is more reasonable than the Freundlich model in describing the process, which also indicates that the change of particle size doesn't bring effects on the monolayer adsorption nature of MB or NH_4^+ onto STs and PSTs [47, 48].

Table 2. Isotherm parameters of NH_4^+ or MB adsorption onto STs and PSTs.

Adsorbates	Samples	Langmuir model			Freundlich model		
		Q_{max}/mg·g^{-1}	K_L/L·mg^{-1}	R^2	K_F/(mg$^{(n-1)}$·L)$^{1/n}$·g^{-1}	*1/n*	R^2
MB	ST(1:1)	52.81	0.012	0.9978	3.30	0.46	0.9526
	ST(1:10)	51.76	0.017	0.9875	4.48	0.42	0.9963
	ST(1:20)	58.94	0.013	0.9780	3.76	0.47	0.9750
	PST-5	98.52	0.010	0.9904	3.59	0.56	0.9474
	PST-10	94.47	0.007	0.9943	2.61	0.59	0.9743
	PST-20	98.23	0.007	0.9942	2.13	0.62	0.9602
NH_4^+	ST(1:1)	44.82	0.029	0.9921	3.61	0.50	0.9806
	ST(1:10)	44.48	0.031	0.9888	3.90	0.48	0.9725
	ST(1:20)	45.97	0.032	0.9926	3.93	0.49	0.9776
	PST-5	45.26	0.034	0.9886	4.22	0.48	0.9713
	PST-10	46.18	0.027	0.9916	3.40	0.51	0.9773
	PST-20	42.91	0.028	0.9942	3.26	0.51	0.9747

3.3.3. Adsorption kinetics

The kinetic experiment was conducted to find the relationship between particle size and adsorption kinetics, and the results of the experiments are shown in Fig. 3. It is illustrated that samples with smaller particle sizes can reach the adsorption equilibrium of either NH_4^+ or MB more quickly than those with a bigger size. For

example, the adsorption of MB onto ST(1:20) (D_{50}= 53.56 μm) can be finished within 10 min, which is shorter than the 60 min of ST(1:10) (D_{50}= 72.78 μm) and 90 min of ST(1:1) (D_{50}= 89.13 μm) at the same conditions. Thus, the effect of particle size on the equilibrium time was independent of the adsorbate species. In addition, two typical kinetic models (pseudo-first-order and pseudo-second-order models) were used to fit the experimental data to find the effect of particle size on the kinetic nature of the adsorption process. The fitting curves are shown in Fig. 3, and the related parameters are listed in Table S1. The value of kinetic constants (K_1 and K_2) of the two models indicate the order of adsorption rate values as ST(1:20)> ST(1:10)> ST(1:1) and PST-5> PST-10> PST-20. The value of correlation coefficient R^2 indicates that the pseudo-second-order model is more suitable for describing the kinetic adsorption process of both NH_4^+ and MB onto the as-prepared samples, which further demonstrates that the difference in particle size doesn't have a pronounced effect on the chemisorption nature of the kinetic process.

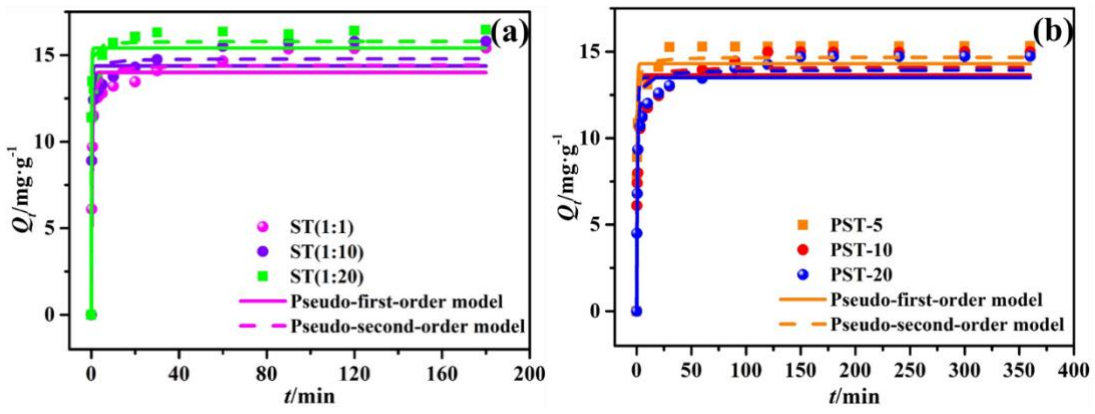

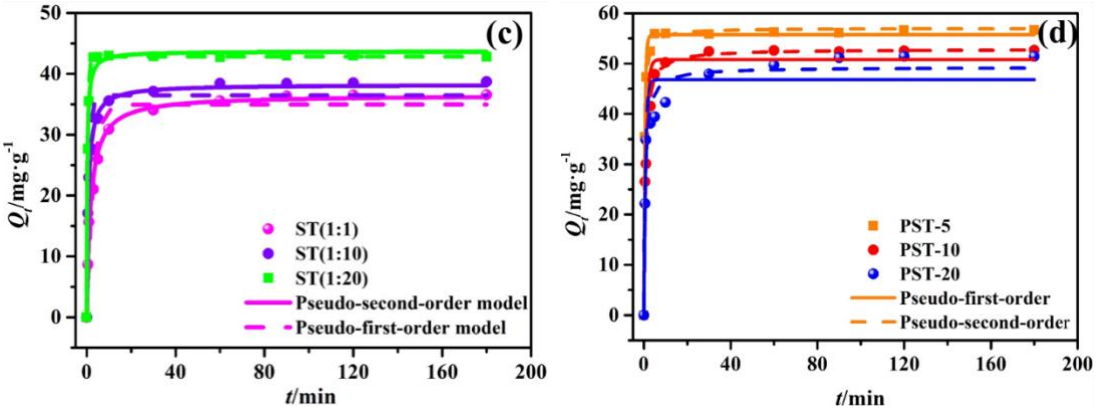

Figure 3. Adsorption kinetics of NH_4^+ onto STs (a), PSTs (b) and MB onto STs (c), PST(d). (Experimental conditions: C_0= 45 mg·L^{-1} for NH_4^+ and 275 mg·L^{-1} for MB; initial solution pH=7)

It is also illustrated from the experimental data that samples with smaller sizes could adsorb pollutants more quickly than those with bigger sizes at the beginning short time, which reveals that the size value of particles can significantly affect the adsorption rate at the primary stage. Therefore, the Elovich model was also employed to fit the experimental data, as shown in Fig. 4 and Table S2. It is evident that the value of α (initial adsorption rate) of STs and PSTs in adsorption of MB and NH_4^+ are all in the order of PST-5> PST-10> PST-20 and ST(1:20)> ST(1:10)> ST(1:1), which is opposite to the order of secondary particle size. The above results demonstrate that the effect of particle size on the difference of adsorption rate mainly occurs at the very early time when samples just in contact with the solution.

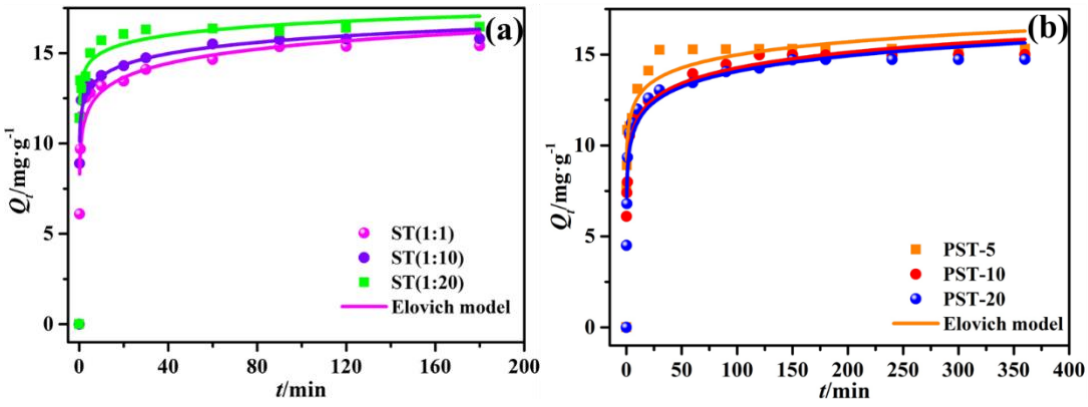

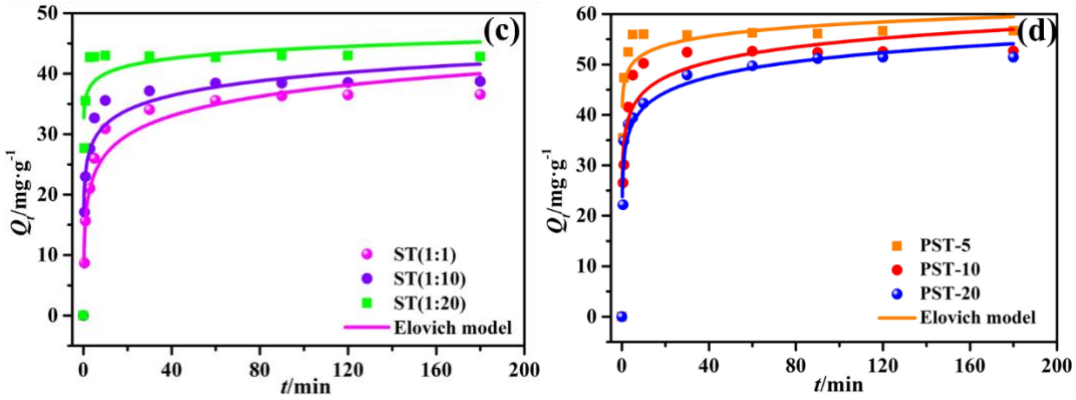

Figure 4. The fitting results of adsorption of NH_4^+ onto STs (a), PSTs (b) and adsorption of MB onto STs (c), PSTs (d) by Elovich model.

The entire aqueous adsorption process usually contains three stages: liquid film diffusion, intraparticle diffusion and internal adsorption reaction [32]. In the early time of the adsorption process, adsorbate molecules can move to the surface of sample particles and enter into the internal framework through liquid film diffusion. The decrease of particle size would make adsorbent powders diffuse more easily and quickly in the solution and reduce the liquid film thickness, which successfully accelerated the initial adsorption stage [49]. To make sure that the liquid film diffusion process is one of the rate-limiting steps in the adsorption of NH_4^+ or MB onto STs and PSTs, the Weber-Morris model was used to fit the experimental data as shown in Fig. 5 and Table S3. The fitting curves don't cross the origin, and the value of *C* are all bigger than zero, which indicates that intraparticle diffusion is not the only rate-limiting step. The whole adsorption rate is controlled by multiple diffusion modes [50]. Therefore, the effect of particle size on the liquid film diffusion process can affect the adsorption rate to some extent, especially at the early contact time.

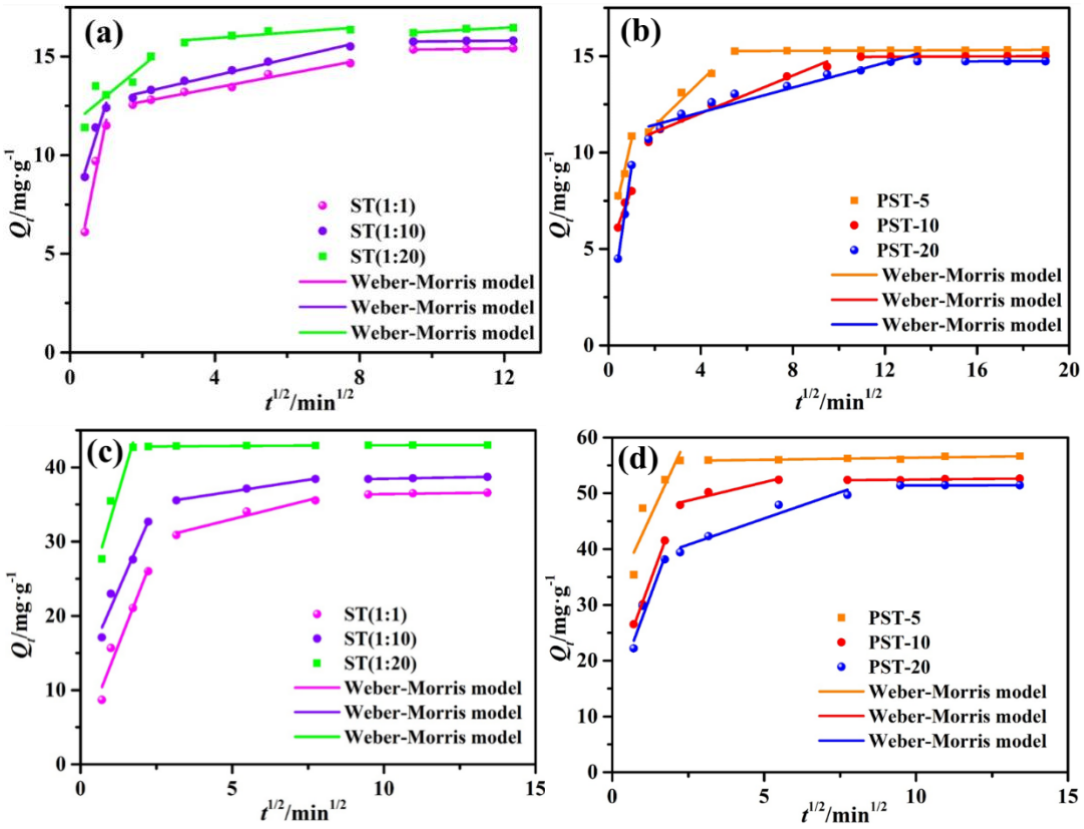

Figure 5. Adsorption kinetics of NH_4^+ (a, b) and MB (c, d) onto samples with the fitting of the Weber-Morris model.

Therefore, the regulation of secondary size value can be carried out to improve the separation ability and adsorption kinetics for the powder-shape adsorbent. The enhancement of sedimentation ability can increase the separation efficiency and reduce the relative cost for recovering the exhausted adsorbents. However, the larger secondary size would mean more prolonged adsorption kinetics and finally reduce the adsorption efficiency. A balance or a key point should be found between these two opposite results. Therefore, an entire cost calculation is suggested to help determine the secondary size value when designing adsorbent materials in the actual application. The investigation of this issue will be focused on in future studies.

4. Conclusions

In this study, a series of sodium titanates (STs) and peroxide modified sodium

titanates (PSTs) particles with different sizes were synthesized through the control of hydrolysis and complexation by changing the ratio of reagents. The as-prepared samples were applied in the adsorption of NH_4^+ and MB from an aqueous solution to figure out the effect of particle size on the adsorbent properties and adsorption performance. The sedimentation experiment and CFD simulation indicated that the change of secondary size (particles size after agglomeration, aggregation or hydration in solution) could effectively affect the settling ability of adsorbent powders, which is meaningful for regulating the separation ability of adsorbent materials. In addition, the effect of secondary size on adsorption kinetics is also non-negligible. The PSTs or STs particles with smaller secondary sizes can reach adsorption equilibrium for NH_4^+ and MB more quickly than those with a bigger size. The fitting results from Elovich and Weber-Morris models demonstrate that the particles size affect kinetics mainly in the liquid film diffusion process at the early contact time. Therefore, the secondary size significantly affects the sedimentation ability and adsorption kinetics of titanate-based adsorbents in the opposite results, which is helpful for adsorbent design and mechanism analysis.

Acknowledgements

This research is supported by the National Natural Science Foundation of China (NO. 52070155 and NO. 51978569).

Appendix A. Supplementary data

Eqs. (S1)- (S2): Langmuir and Freundlich models
Eqs. (S3)- (S4): Pseudo-first order and Pseudo-second models.
Eqs. (S5)- (S6): Elovich model and Web-morris model

References

[1] P.A. Wosiack, D.D. Lopes, M.H. Rissato Zamariolli Damianovic, E. Foresti, D. Granato, A.C. Barana, J. Environ. Manage. 154 (2015) 145-150.
[2] X. Liu, Y. Zhang, X. Li, C. Fu, T. Shi, P. Yan, Sci. Total Environ. 635 (2018) 1360-1366.
[3] P. Zhang, X. Zeng, X. Wen, C. Yang, S. Ouyang, P. Li, Z. Gu, D. Wu, R.L. Frost, Chem. Eng. J. 366 (2019) 11-20.
[4] G.z. Xin, M. Wang, L. Chen, Y. Zhang, M. Wang, W. Jiang, Y. Chen, RSC Advances 9 (2019) 6452-6459.
[5] M.T. Yagub, T.K. Sen, S. Afroze, H.M. Ang, Adv. Colloid Interface Sci. 209 (2014) 172-184.
[6] A.J. Howarth, M.J. Katz, T.C. Wang, A.E. Platero-Prats, K.W. Chapman, J.T. Hupp, O.K. Farha, J. Am. Chem. Soc. 137 (2015) 7488-7494.
[7] L. Gao, C.Y. Zhang, Y. Sun, C. Ma, Environ. Technol. 40 (2019) 1959-1968.
[8] J.W. Fu, Z.H. Chen, M.H. Wang, S. Liu, J. Zhang, J. Zhang, R. Han, Q. Xu, Chem. Eng. J. 259 (2015) 53-61.
[9] K. Wu, Y. Li, T. Liu, N. Zhang, M. Wang, S. Yang, W. Wang, P. Jin, Environ. Sci. Pollut. Res. 26 (2019) 17632-17643.
[10] D. Guaya, C. Valderrama, A. Farran, C. Armijos, J.L. Cortina, Chem. Eng. J. 271 (2015) 204-213.
[11] Y. Li, X. Yin, X. Huang, J. Tian, W. Wu, X. Liu, Appl. Surf. Sci. 495 (2019) 143626.
[12] L. Wang, J. Wang, W. Yan, C. He, Y. Shi, Chem. Eng. J. 387 (2020) 123305.
[13] Q. Xiao, Y. Sun, J. Zhang, Q. Li, Appl. Surf. Sci. 356 (2015) 18-23.
[14] C.D. Walkey, J.B. Olsen, H. Guo, A. Emili, W.C. Chan, J. Am. Chem. Soc. 134 (2012) 2139-2147.
[15] Z. Wang, M. Song, C. Sun, Y. He, Mater. Sci. Eng., A 528 (2011) 1131-1137.

[16] T.M. Berhane, J. Levy, M.P.S. Krekeler, N.D. Danielson, Appl. Clay Sci. 132-133 (2016) 518-527.
[17] M.A. Al-Ghouti, M.A. Khraisheh, M.N. Ahmad, S. Allen, J. Hazard. Mater. 165 (2009) 589-598.
[18] N.T. Thanh, N. Maclean, S. Mahiddine, Chem. Rev. 114 (2014) 7610-7630.
[19] V.H. Grassian, J. Phys. Chem. C 112 (2008) 18303-18313.
[20] M. Motlochová, V. Slovák, E. Pližingrová, S. Lidin, J. Šubrt, RSC Advances 10 (2020) 3694-3704.
[21] A.A. Farghali, A.H. Zaki, M.H. Khedr, Nanomaterials and Nanotechnology 6 (2016) 1-6.
[22] W.L. Zhang, R. Fu, L. Wang, J.W. Zhu, J.T. Feng, W. Yan, Sci. Total Environ. 668 (2019) 815-824.
[23] M. Feng, W. You, Z.S. Wu, Q. Chen, H. Zhan, ACS Applied Materials Interfaces 5 (2013) 12654-12662.
[24] Y. Zhang, G. Li, J. Liu, T. Wang, X. Wang, B. Liu, Y. Liu, Q. Huo, Z. Chu, J. Colloid Interface Sci. 528 (2018) 109-115.
[25] R. Saleh, A.H. Zaki, F.I.A. El-Ela, A.A. Farghali, M. Taha, R. Mahmoud, J. Environ. Chem. Eng. 9 (2021) 104726.
[26] D.H. Chen, L. Cao, F.Z. Huang, Paolo Imperia, Yi-Bing Cheng, R.A. Caruso, J. Am. Chem. Soc. 132 (2010) 4438-4444.
[27] N.A.M. Barakat, A.H. Zaki, E. Ahmed, A.A. Farghali, F.S. Al-Mubaddel, Int. J. Hydrogen Energy 43 (2018) 7990-7997.
[28] M.S. Mahmoud, E. Ahmed, A.A. Farghali, A.H. Zaki, E.A.M. Abdelghani, N.A.M. Barakat, Colloids Surf., A 554 (2018) 100-109.
[29] P. Song, J.J. Sun, C.J. Huo, Int. J. Refrig. 108 (2019) 60-78.
[30] D. Cidaspow, J. Ding, AlChE J. 36 (1990) 523-538.
[31] K.Y. Foo, B.H. Hameed, Chem. Eng. J. 156 (2010) 2-10.
[32] H. Qiu, L. Lv, B.C. Pan, Q.J. Zhang, W.M. Zhang, Q.X. Zhang, J. Zhejiang Univ.-SCI A 10 (2009) 716-724.
[33] Y.S. Ho, J. Hazard. Mater. 136 (2006) 681-689.
[34] A. Zaban, S.T. Aruna, S. Tirosh, B.A. Gregg, Y. Mastai, J. Phys. Chem. B 104 (2000) 4130-4133.
[35] M.C. Surette, J.A. Nason, Environ.-Sci. Nano 6 (2019) 540-553.
[36] J. Muehlebach, K. Mueller, G. Schwarzenbach, Inorg. Chem. 9 (1970) 2381-2390.
[37] K. Kiatkittipong, C.H. Ye, J. Scott, R. Amal, Cryst. Growth Des. 10 (2010) 3618-3625.
[38] D. Magri, G. Caputo, G. Perotto, A. Scarpellini, E. Colusso, F. Drago, A. Martucci, A. Athanassiou, D. Fragouli, ACS Applied Materials Interfaces 10 (2018) 651-659.
[39] X. Kong, C. Zeng, X. Wang, J. Huang, C. Li, J. Fei, J. Li, Q. Feng, Scientific Reports 6 (2016) 29049.
[40] Q. Gao, J. Xu, X.H. Bu, Coord. Chem. Rev. 378 (2019) 17-31.
[41] W. Lyu, J.M. Wu, W.L. Zhang, Y.P. Liu, M.T. Yu, Y.F. Zhao, J.T. Feng, W. Yan, Chem. Eng. J. 363 (2019) 107-119.
[42] S. Balachandar, J.K. Eaton, Annu. Rev. Fluid Mech. 42 (2010) 111-133.
[43] C. Bechinger, R.D. Leonardo, H. Löwen, C. Reichhardt, G. Volpe, G. Volpe, Rev. Mod. Phys. 88 (2016) 045006.

[44] S.M. Prabhu, C.M. Park, A. Shahzad, D.S. Lee, J. Mater. Chem. A. 7 (2019) 12253-12265.
[45] K.S.D. Premarathna, A.U. Rajapaksha, B. Sarkar, E.E. Kwon, A. Bhatnagar, Y.S. Ok, M. Vithanage, Chem. Eng. J. 372 (2019) 536-550.
[46] L. Huang, L. Li, W.B. Dong, Y. Liu, H.Q. Hou, Environ. Sci. Technol. 42 (2008) 8070-8075.
[47] X.Y. Wan, Y.Q. Zhan, Z.H. Long, G. Zeng, Y. He, Chem. Eng. J. 330 (2017) 491-504.
[48] S. Xue, X.B. Zhang, H.H. Ngo, W.S. Guo, H.T. Wen, C.C. Li, Y.C. Zhang, C.J. Ma, Bioresour. Technol. 292 (2019) 121927.
[49] S.S. Gupta, K.G. Bhattacharyya, Adv. Colloid Interface Sci. 162 (2011) 39-58.
[50] A.C. Martins, O. Pezoti, A.L. Cazetta, K.C. Bedin, D.A.S. Yamazaki, G.F.G. Bandoch, T. Asefa, J.V. Visentainer, V.C. Almeida, Chem. Eng. J. 260 (2015) 291-299.